Asian Journal of Pharmaceutical Sciences 14 (2019) 531–542

Available online at www.sciencedirect.com

ScienceDirect

journal homepage: www.elsevier.com/locate/AJPS

Original Research Paper

Redox-sensitive micelles for targeted intracellular delivery and combination chemotherapy of paclitaxel and all-trans-retinoid acid

Lingfei Han[b,1], *Lejian Hu*[a,1], *Fulei Liu*[a], *Xin Wang*[b], *Xiaoxian Huang*[a], *Bowen Liu*[a], *Feng Feng*[a,c], *Wenyuan Liu*[b,d,*], *Wei Qu*[a,*]

[a] *Department of Natural Medicinal Chemistry, China Pharmaceutical University, Nanjing 210009, China*
[b] *Department of Pharmaceutical Analysis, China Pharmaceutical University, Nanjing 210009, China*
[c] *Jiangsu Food and Pharmaceutical Science College, Huaian 223003, China*
[d] *Key Laboratory of Drug Quality Control and Pharmacovigilance, Ministry of Education, China Pharmaceutical University, Nanjing 210009, China*

ARTICLE INFO

Article history:
Received 24 June 2018
Revised 7 August 2018
Accepted 17 August 2018
Available online 24 September 2018

Keywords:
Redox-sensitive
Hyaluronic acid
All-trans-retinoid acid
Tumor targeting
Combination chemotherapy

ABSTRACT

The application of paclitaxel (PTX) in clinic has been restricted due to its poor solubility. Several traditional nano-medicines have been developed to improve this defect, while they are still lack of tumor targeting ability and rapid drug release. In this work, an amphiphilic polymeric micelle of hyaluronic acid (HA) – all-trans-retinoid acid (ATRA) with a disulfide bond, was developed successfully for the co-delivery of PTX and ATRA. The combination chemotherapy of PTX and ATRA can strengthen the anti-tumor activity. Along with self-assembling to micelles in water, the delivery system displayed satisfying drug loading capacities for both PTX (32.62% ± 1.39%) and ATRA, due to directly using ATRA as the hydrophobic group. Rapid drug release properties of the PTX-loaded redox-sensitive micelles (HA-SS-ATRA) *in vitro* were confirmed under reducing condition containing GSH. Besides, HA-CD44 mediated endocytosis promoted the uptake of HA-SS-ATRA micelles by B16F10 cells. Due to these properties, cytotoxicity assay verified that PTX-loaded HA-SS-ATRA micelles showed concentration-dependent cytotoxicity and displayed obvious combination therapy of PTX and ATRA. Importantly, HA-SS-ATRA micelles could remarkably prolong plasma circulation time after intravenously administration. Therefore, redox-sensitive HA-SS-ATRA micelles could be utilized and explored as a promising drug delivery system for cancer combination chemotherapy.

* Corresponding authors. China Pharmaceutical University, No. 639, Longmian Road, Nanjing 211198, China. Tel.: +86 13851630593.
E-mail addresses: liuwenyuan8506@163.com (W. Liu), popoqzh@126.com (W. Qu).
[1] Both authors contributed equally to this work.
Peer review under responsibility of Shenyang Pharmaceutical University.

https://doi.org/10.1016/j.ajps.2018.08.009

1. Introduction

Cancer is an important type of the intractable health problems all over the world. Chemotherapy, as an effective treatment, is still playing a significant role so far. However, single drug therapy is not enough to meet the requirements of the treatment of complex cancers and may lead to drug resistances. Nowadays, cancer combination chemotherapy has drawn wide attention to overcome drug resistance and maximize the therapeutic effect by modulating different signaling pathways of cancer [1,2]. Consequently, it posed a problem how to improve the compliance of patients with multiple drugs to take.

Considering this issue, to combine two drugs in one drug delivery system may be a good idea. In our study, two drugs used for combination chemotherapy are paclitaxel (PTX) and all-trans-retinoid acid (ATRA). PTX is a classic natural antimicrotubule drug showing a wide range of antitumor activity spectrum against various cancer diseases like lung cancer, leukemia, metastatic and refractory breast cancer as well as ovarian cancer [3]. Currently, a few drugs such as topotecan, cisplatin, S-1, 5-fluorouracil and carboplatin have been applied together with PTX for several cancer combination chemotherapy [4–7]. Among them, ATRA, a derivative of vitamin A, which could promote cell apoptosis and induce differentiation in leukemia and glioblastoma cells [8], can reduce survivin expression in MCF-7 cells and thus enhancing PTX-induced cytotoxicity [9]. Kamakar et al. found combination therapy of ATRA and PTX could suppress several cell survival factors by down-regulating NF-κB and BIRC and proteins promoting phosphorylation of Bcl-2 [10]. However, both PTX and ATRA are water-insoluble, which is unfavorable for the intravenous injection in cancer therapy. Therefore, it is necessary to solve the barriers, which may hinder simultaneously delivering of PTX and ATRA [11].

Polymeric micelles are widely applied as a class of drug delivery system for its tremendous potential in cancer therapy. It has many advances such as increasing the solubility and stability of anticancer drugs, prolonging its blood circulation cycle and achieving passive targeting with suitable sizes through the enhanced permeability and retention (EPR) effect [12]. However, the traditional nanomedicines based on biodegradable polymers usually exhibit slow degradation behavior *in vivo*, which may bring inadequate drug release and weakened treatment efficacy [14,15]. Besides, delivering drug molecules only through passive targeting might not be enough with low treatment efficacy and potential side effects [13]. Recent studies indicate that, it is more desirable to achieve accurately tumor targeting and rapid drug release for enhanced therapeutic efficacy [16]. Thus, two strategies aimed at these goals were applied in this study.

The first is to introduce a sensitive bond, which could be triggered by tumor microenvironment to accelerate the drug release. Recently, numerous micelles with the function of redox-sensitivity have been designed for their immediate drug release triggered by the intracellular reducing molecules such as glutathione (GSH) [17]. Disulfide bonds are such a linker, which are stable in blood but sensitive and cleavable by thiol-disulfide interchange when exposed to GSH [18,19]. As is well known, tumor cells expressed much more GSH than plasma (2.0–20.0 μM) and normal cells (0.5–10.0 mM) [20–23]. Hence, exploiting the unique intracellular redox potential of tumor tissues could be the strategy of designing micelles with specific and rapid release properties.

The second is to introduce an active targeting ligand, which could target receptors overexpressing on tumor cells. Hyaluronic acid (HA) is a natural biocompatible polyanionic polysaccharide [24], which has recently attracted extensive attention for its considerable physiological properties like biocompatibility, biodegradability, no immunogenicity [25], high affinity to CD44 receptor and RHAMM receptor, which overexpressed on several malignant tumors [26–29], and multiple modification sites. For example, Li et al. successfully developed an amphiphilic hyaluronic acid-deoxycholic acid (HA-DOCA) micelle for tumor targeting delivery of PTX [30]. Similarly, Yao et al. synthesized an amphiphilic HA-ATRA conjugate through a pH-sensitive amido bond as a tumor targeting nanocarrier for PTX [31]. These blank materials all showed little toxicity to normal and tumor cells.

Herein, we developed a novel design of redox-sensitive micelles with active targeting ability based on HA-SS-ATRA conjugates. We make use of the ATRA as a part of drug carriers to encapsulate PTX in the inner core of micelles, thus achieving their co-delivery for combination cancer chemotherapy. What's more, since ATRA directly functioned as the hydrophobic group of the micelles, it will certainly increase the drug loading capacity. As illustrated in Fig. 1, the constructed self-assembly HA-SS-ATRA micelles show good stability in blood matrixes. It could permeate into tumor site via EPR effect and be selectively and efficiently taken up through HA-receptors mediated endocytosis. Once stimulated by the redox environment in tumor cytoplasm, the micelles could achieve rapid disassembly, thereby accelerating the drug release and improving the antitumor efficiency.

2. Materials and methods

2.1. Materials and cell cultures

Sodium hyaluronic acid (MW 15 kDa) was purchased from Dong Yuan Biotech Co., Ltd. (Jiangsu, China). Tetrabutylammonium hydroxide (TBA-OH), phosphorus tribromide, 1, 6-dibromohexane, nile red (NR) and GSH were purchased from Aladdin Reagent Database Inc. (Shanghai, China). ATRA and bis (2-hydroxyethyl) disulfide were purchased from Energy Chemical (Shanghai, China). PTX was purchased from Sinopharm Chemical Reagent Co., Ltd. (Shanghai, China).

B16F10 and L929 cells were purchased from the cell bank of Chinese Academy of Sciences. The cells were cultured in DMEM with 10% (v:v) FBS in an incubator (ESCO, Singapore) at 37 °C under 5% CO_2.

2.2. Synthesis of HA-SS-ATRA conjugate and HA-ATRA conjugate

2.2.1. Synthesis of HA-TBA

Hyaluronic acid (HA, 24.4 mmol) and tetra-n-butyl ammonium hydroxide (TBA, 19.4 mmol) were together added to 60 ml of

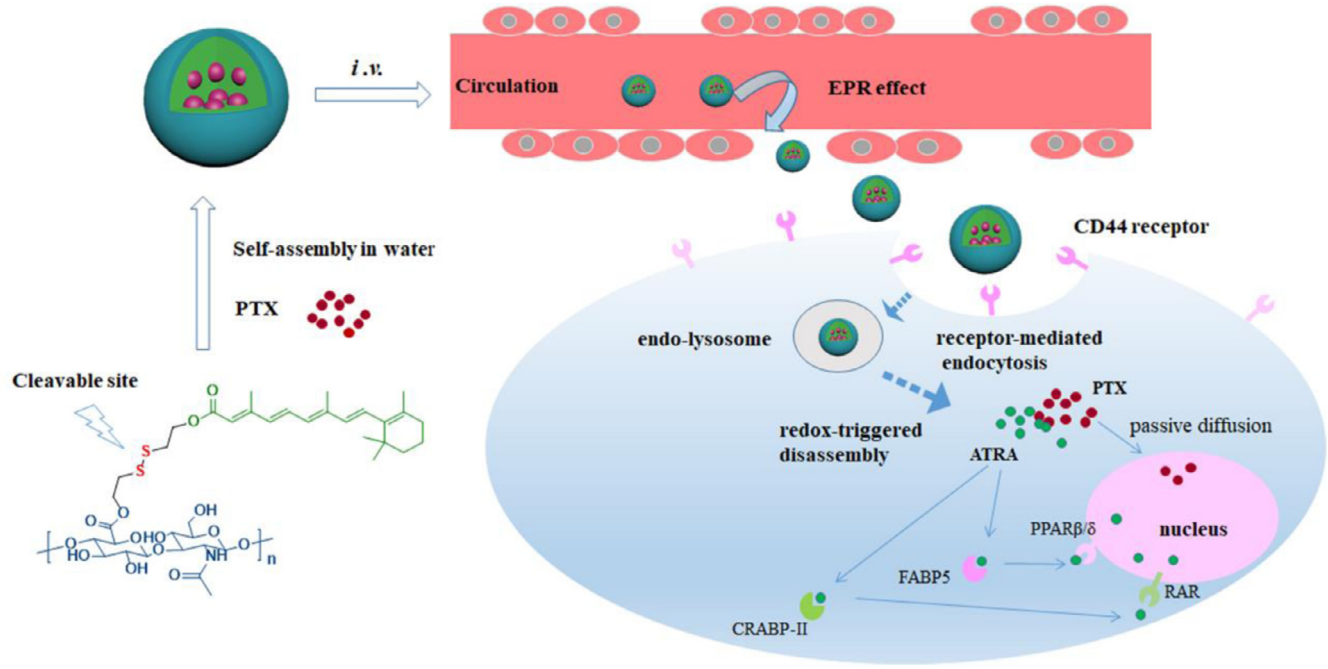

Fig. 1 – Illustration of the self-assembly, accumulation at tumor tissue, receptor-mediated endocytosis, intracellular the redox-triggered disassembly and two drugs release mechanism.

distilled water and stirred for 60 min. Then, gather the activated HA-TBA salt after freeze drying [25].

2.2.2. *Synthesis of HA-SS-ATRA conjugate and HA-ATRA conjugate*

A solution of PBr_3 (0.246 ml, 2.6 mmol) in DCM (5 ml) was added to a solution of Bis (2-hydroxyethyl) Disulfide (0.4 g, 2.6 mmol) in dichloromethane (DCM, 20 ml), and the mixture was stirred for 15 h. The reaction was terminated by the addition of water and with DCM extraction. After chromatographic purification, 0.33 g (55.3%) of **1** was obtained.

To synthesize the HA-SS-ATRA conjugate and HA-ATRA conjugate, ATRA (17.18 mmol), triethylamine (18.90 mmol) in 50 ml of tetrahydrofuran (THF) and **1** or 1,6-dibromohexane (17.18 mmol) in 20 ml of THF were mixed, respectively. After 3 h of stirring at room temperature, the **2** and **3** was obtained by chromatographic purification. HA-TBA and **2** or **3**, which the molar ratio of ATRA to sugar residues of HA varied from 1:10 to 10:10, were solubilized in DMSO and stirred for 48 h at 50 °C, the resulting solution was precipitated in acetone, dialyzed against the excess amount of **2** with NaCl solution (5%, w/v) and distilled water, respectively. After freeze-drying, the white powders were obtained and preserved at 4 °C until ready for use. (**1**, **2**, **3** were compounds seen in Fig. 2.)

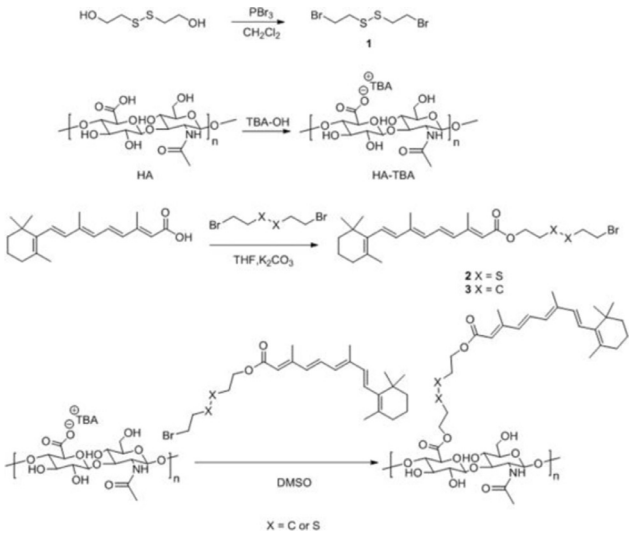

Fig. 2 – Synthetic scheme of HA-SS-ATRA conjugates and HA-ATRA conjugates.

2.3. *Characterization of HA-SS-ATRA conjugates and HA-ATRA conjugate*

The chemical structures of the HA-SS-ATRA, HA-ATRA conjugates were confirmed by ^{1}H NMR at 300 MHz (AVACE, Bruker), IR (Tensor 27, Bruker) and UV (T6, Purkinje). The degree of substitution (DS), representing the molar ratio of ATRA and HA, was determined by UV spectrometry of ATRA in DMSO ($\lambda = 348$ nm).

2.4. *Preparation and characterization of micelles*

A preparation method of the redox-sensitive HA-SS-ATRA micelles was described as follows: 40 mg of HA-SS-ATRA conjugates were dissolved in 6 ml of distilled water with sonication for 30 min (VCX500, Sonics) in the ice bath. The control group of non-redox-sensitive HA-ATRA micelle were prepared in the same way.

The prepared micelles were firstly characterized from the particle size and zeta potential by means of dynamic light scattering (DLS) using a Malvern Zetasizer Nano-ZS90 (Malvern Instruments) and transmission electron microscopy (TEM, Tecnai, Philips company).

Then, an important parameter for micelles, critical micelle concentration (CMC) values of HA-SS-ATRA conjugates and HA-ATRA conjugate in distilled water were measured applying the classic fluorescence pyrene method. Briefly, aliquots of 6.0 nmol pyrene were put into a series of 10 ml of volumetric flasks and bring to volume with several concentration gradients of HA-SS-ATRA conjugates or HA-ATRA conjugate solutions (0.1–200 μg/ml). After 30 min of sonicating, the fluorescence spectrum charts were depicted with a Fluoromax-4 florescence spectrophotometer (HORIBA Scientific) with the excitation wavelength at 336 nm. The CMC value was estimated through curve-fitting to find the cross-point from extrapolating the fluorescence intensity ratio of I372/I392.

2.5. *Reduction-triggered disassembly of blank micelles by GSH*

The sensitivity of HA-SS-ATRA micelles to the reducing environment was observed through incubation at 20 mM GSH for different time (0, 1, 3, 6, 9, 12 h) in PBS (pH 7.4, 10 mM) at 37 °C. The solution was shaken at 37 °C and the size distribution of micelles was measured by DLS at predetermined time intervals. The size change of non-redox-sensitive HA-ATRA micelles were also measured as control.

2.6. *Preparation and characterization of PTX-loaded micelles*

PTX-loaded HA-SS-ATRA (HA-SS-ATRA/PTX) micelles and PTX-loaded HA-ATRA (HA-ATRA/PTX) micelles were prepared using a dialysis method. Briefly, 20 mg of HA-SS-ATRA conjugate or HA-ATRA conjugate was dissolved in 3 ml of distilled water followed by 30 min of stirring. Then, the conjugate solution was added dropwise a total weight of 10 mg PTX dissolved into 30 mg/ml anhydrous ethanol solution, followed by 30 min of sonication by probe-type ultrasonicator. The solution was dialyzed with distilled water in a dialysis bag (MWCO 5000) for 24 h, then centrifugated at 4000 rpm for 5 min to remove the unloaded PTX. The supernatant was collected and freeze-dried to obtain the final PTX-loaded micelles.

To establish a content analysis method for PTX, the micelles was extracted with five-fold volume of methanol, then filtered with a 0.22 μm membrane and injected into HPLC (Primaide, HITACHI) with UV detection at 227 nm. PTX was isocratically eluted under methanol: $H_2O = 65{:}35$ (v/v) using the ODS column (4.6 mm × 250 mm, 5 μm) at the flow rate of 1 ml/min. The encapsulation efficiency (EE) and drug loading (DL) of PTX were calculated as follows:

$$EE(\%) = \frac{\text{weight of PTX in micelles}}{\text{weight of PTX fed initially}} \times 100\%$$

$$DL(\%) = \frac{\text{weight of PTX in micelles}}{\text{weight of PTX in micelles} + \text{weight of conjugates fed intially}} \times 100\%$$

Also, DLS and TEM were applied to observe the morphology, size and zeta of PTX-loaded micelles. In addition, to confirm the complete encapsulation of PTX in the micelles, X-ray diffraction (XRD) spectrometry was scanned in a powder diffraction meter (AXS, Bruker). The scanning mode was set including scanning range (0°–50° (2 u)), speed (1°/min), step (0.05° (2 u)), current (40 mA) and potential (40 kV).

2.7. *In vitro release of PTX and ATRA from micelles triggered by GSH*

The *in vitro* release profiles of PTX and ATRA from the HA-SS-ATRA/PTX micelles were carried out using the modified dialysis. Micelles were resuspended in PBS and added into a dialysis bag (MWCO 5000 Da), with 100 ml of PBS (10 mM, pH 7.4, 0.1% Tween80; w:v) containing different concentrations of GSH (0 μM, 10 μM, 10 mM and 20 mM) as the release medium. All samples were softly shaken at 100 rpm at 37 °C. At certain time points, 10 ml of release media was taken out and supplemented the same volume. The drug release profiles of HA-ATRA micelles exposed to 20 mM GSH were also measured as control. All samples were prepared in triplicate.

2.8. *Cellular uptake studies*

The intracellular uptake of the micelles was observed via a fluorescent inverted microscope using a fluorescence marker NR. 0.2% drug loading (150 ng/ml) of NR was loaded in micelles using the same preparation protocol. B16F10 (CD44-positive) and L929 cells (CD44-negative) were cultured with DMEM containing 10% FBS for 24 h. Then, 2 ml of free NR and NR-loaded micelles were replaced the medium. After incubated at 37 °C for 1, 4 and 8 h, the culture media was removed and washed by PBS thrice. To confirm whether micelles were selectively taken up by B16F10 cells through HA-receptor mediated endocytosis, cells were pre-incubated with free HA (10 mg/ml) for 2 h before the HA-SS-$ATRA_{21}$/PTX micelles (10 μg/ml) being added. Furthermore, HA-receptor mediated endocytosis was confirmed by L929 cells. Finally, all samples were washed by PBS thrice and observed via a fluorescent inverted microscope.

In addition, to preciously quantify the difference of cellular uptake, a flow cytometer (FCM) was conducted. B16F10 cells and L929 cells were cultured and treated as described above. After 1 and 4 h of incubation, operations were performed in the following turn: wash with PBS thrice, harvest with trypsinization, resuspend with PBS and measure at fluorescent detection wavelength 560/620 nm.

2.9. *In vitro cytotoxicity activity studies*

The *in vitro* cytotoxicity of HA-SS-$ATRA_{21}$/PTX, HA-$ATRA_{20}$/PTX, PTX and PTX + ATRA against the B16F10 and L929 cells were evaluated by the MTT assay. B16F10 and L929 cells were seeded into 96-well plates at a density of 5.0×10^3 cells per well and incubated for 24 h at 37 °C with 5% CO_2. The growth medium was replaced with 100 μl of medium containing HA-SS-$ATRA_{21}$/PTX, HA-$ATRA_{20}$/PTX, PTX and PTX + ATRA at concentrations ranging from 0.001 to 10 μg/ml. The CD44 receptor of the cells (B16F10) was saturated with free HA

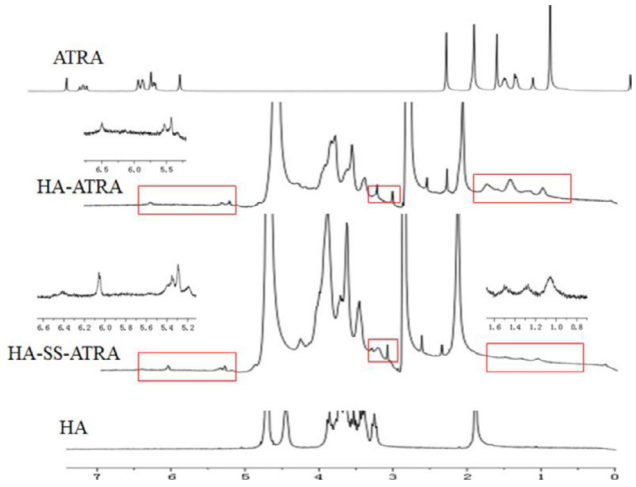

Fig. 3 – ^{1}H NMR spectra of ATRA, HA-ATRA$_{20}$ conjugate, HA-SS-ATRA$_{21}$ conjugate and HA.

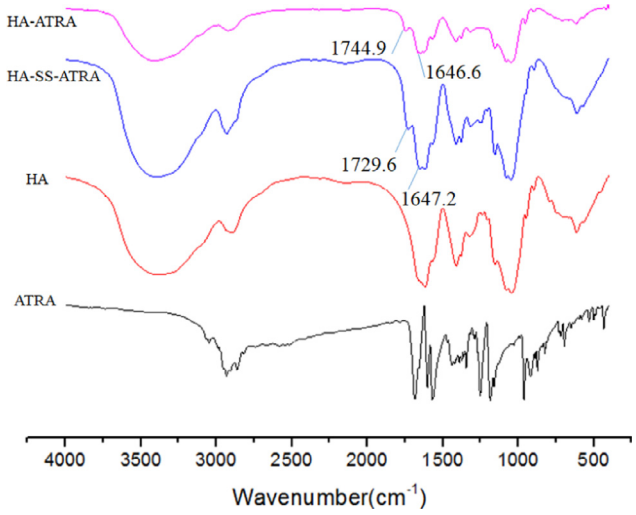

Fig. 4 – FTIR spectra of HA-SS-ATRA$_{21}$ conjugate, HA-ATRA$_{20}$ conjugate, HA and ATRA.

(10 mg/ml) for 2 h before HA-SS-ATRA$_{21}$/PTX (10 μg/ml) treatment, and then the cells were washed with PBS. The blank culture medium was used as control. After further incubation for 48 h, MTT assay was conducted.

2.10. *Pharmacokinetics*

Sprague–Dawley rats (200 ± 20 g, male) were purchased from Yangzhou University (Yangzhou, China). The animal experiments were performed under the guidelines of the Animal Ethics Committee of China Pharmaceutical University (Nanjing, China). Healthy male Sprague–Dawley rats (200± 20 g) were randomly divided into three groups (n = 5). Taxol®, HA-SS-ATRA$_{21}$/PTX and HA-ATRA$_{20}$/PTX were intravenously administered through the tail vein at an equivalent dose of PTX (7 mg/kg body weight). Blood sample (about 0.3 ml) were collected at predetermined time points of 5 min, 10 min, 15 min, 30 min, 1 h, 2 h, 4 h, 6 h, 8 h, 12 h, 24 h and 48 h into heparinized tubes and centrifuged at 8000 rpm for 10 min, then stored at −20 °C until analysis. 10 μl of diazepam, as the internal standard, was added into 75 μl of plasma and vortexed for 1 min, and 750 μl of methyl tert-butyl ether was further added and vortexed for 10 min. Then, after centrifuging at 12 000 rpm for 10 min, the supernatant was separated and evaporated to dryness under nitrogen gas. The residue was reconstituted in 100 μl of methanol and analyzed by HPLC.

3. Results and discussion

3.1. *Synthesis of HA-SS-ATRA and HA-ATRA conjugate*

The amphiphilic polymeric conjugates, HA-SS-ATRA and HA-ATRA, were synthesized as shown in Fig. 2. To increase the DS of ATRA, we make HA-TBA salt to make the reaction in DMSO [27], in which both of HA-TBA and ATRA have a good solubility. Since ^{1}H NMR spectra of ATRA (in $CDCl_3$), HA (in D_2O), HA-SS-ATRA (in D_2O) and HA-ATRA (in D_2O) were shown in Fig. 3. Compared with HA, the peaks of HA-SS-ATRA and HA-ATRA made some differences in ^{1}H NMR due to ATRA and linkers introduced to the system. The peaks for N-acetyl group at 2.0 ppm and the signals at 3.0–4.0 ppm and 4.3–4.5 ppm corresponded to glucosidic protons and anomeric protons of HA skeleton, respectively. In the ^{1}H NMR spectra of HA-SS-ATRA, the characteristic peaks at 5.5–6.5 and 1.0–1.6 ppm were assigned to ATRA, meanwhile, the peaks for methylene of linker at 3.0–3.2 ppm and the same signals of HA were also confirmed. In the ^{1}H NMR spectra of HA-ATRA, the peaks of ATRA and HA also existed, indicating that ATRA was successfully grafted into HA.

IR also demonstrated the synthesis of the conjugates. As shown in Fig. 4, the characteristic peaks in 1744.9/1729.6 cm^{-1} and 1646.6/1647.2 cm^{-1} could be ascribed to the stretching vibration of ester and C=C of ATRA backbones, respectively.

The UV spectra further confirmed the structures of HA-SS-ATRA and HA-ATRA. As depicted in Fig. 5, the characteristic peaks at 250 and 350 nm that belonged to HA and ATRA, respectively, were observed.

3.2. *Preparation and characterization of blank micelles*

CMC values confirmed the self-aggregation ability of HA-SS-ATRA and HA-ATRA. As shown in Table 1, the CMC values for HA-SS-ATRA in DI water decreased when the DS of ATRA increased, HA-SS-ATRA$_{21}$ (the DS of ATRA was 21%) possessed CMC of 8.2 μg/ml, which was low enough that the HA-SS-ATRA$_{21}$ micelle could remain their initial morphology even though diluted before reaching the tumor site [32]. However, when the DS of ATRA increased to 29.6%, the water solubility of conjugates was limited. It could hardly get solved in water and far from the formation of micelles. Herein, we just considered those, which could form the micelles in the following characterization studies. To go on, the particle size of HA-SS-ATRA micelles decreased from 194.9 to 162.4 nm as the DS of ATRA increased from 7.5% to 21.3%, which may result from the increasing hydrophobic interaction between PTX and ATRA and thus forming the closer core. The zeta potential of

Table 1 – Characteristics of HA-SS-ATRA and HA-ATRA micelles (mean ± SD, $n = 3$).

Sample	Feed ratio[a]	DS[b] (%)	CMC (μg/ml)	Size[c] (nm)	PDI[d] (μ_2/Γ^2)	*Zeta* potential (mV)
HA-SS-ATRA$_8$[e]	0.1:1	7.5	40.0	194.9 ± 2.7	0.147 ± 0.014	−31.8 ± 0.9
HA-SS-ATRA$_{14}$[e]	0.2:1	14.2	20.0	177.0 ± 1.9	0.283 ± 0.022	−31.0 ± 1.5
HA-SS-ATRA$_{21}$[e]	0.4:1	21.3	8.2	155.5 ± 2.0	0.222 ± 0.012	−33.8 ± 1.0
HA-SS-ATRA$_{30}$[e]	0.6:1	29.6	–[f]	–	–	–
HA-SS-ATRA$_{36}$[e]	1:1	35.8	–	–	–	–
HA-ATRA$_{20}$[e]	0.4:1	20.4	8.8	162.4 ± 1.9	0.214 ± 0.018	−33.1 ± 1.9

[a] Molar feed ratio of ATRA to sugar residues of HA polymer.
[b] Degree of substitution of ATRA.
[c] Mean diameters of micelles.
[d] Polydispersity index of micelles size.
[e] The number represents the degree of substitution of ATRA.
[f] Limited solubility: only soluble below 0.1 mg/ml due to high loading ATRA.

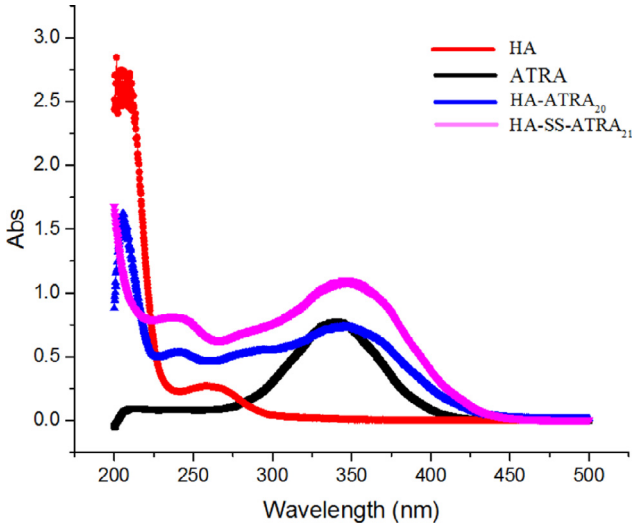

Fig. 5 – Ultraviolet spectra of HA, ATRA, HA-ATRA$_{20}$ and HA-SS-ATRA$_{21}$.

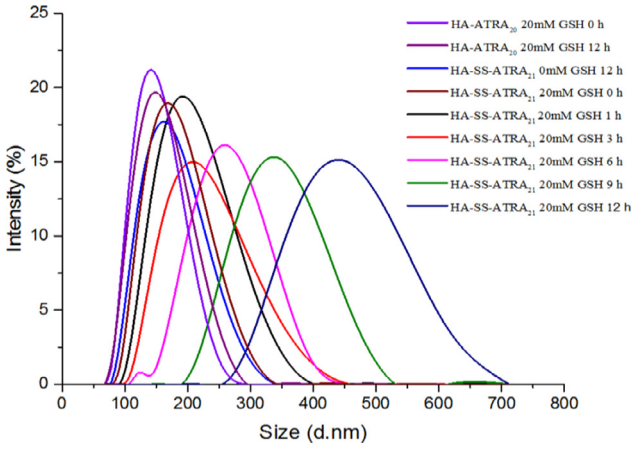

Fig. 6 – Size distribution of HA-SS-ATRA$_{21}$ micelles and HA-ATRA$_{20}$ micelles in response to 20 mM GSH at different time determined by DLS.

HA-SS-ATRA$_{21}$ micelles was −33.8 mV, forming a strong repulsion between micelles and increasing the stability. So, HA-SS-ATRA$_{21}$ micelle became the best choice. In control, the non-redox-sensitive HA-ATRA$_{20}$ micelles were also measured all the data and exhibited similar properties with those of HA-SS-ATRA$_{21}$ micelles due to little difference in composition.

3.3. *Size change of micelles triggered by glutathione*

As is known to all, once the materials of the micelles got damaged, it would lead to the quick disassembly and thus pulling it loose. So, the redox-sensitive function of HA-SS-ATRA$_{21}$ and HA-ATRA$_{20}$ micelles triggered by 20 mM GSH could be evaluated at different time by observing their size change using DLS. As shown in Fig. 6, the average particle size increased from 162.4 nm to 452.1 nm within 12 h. This result confirmed the destruction of the micelles due to cleavage of the disulfide bond. In comparison, no significant change of the size was observed when HA-SS-ATRA$_{21}$ micelles were treated without GSH after 12 h or HA-ATRA$_{20}$ micelles were treated at 20 mM GSH after 12 h. The results indicated that HA-SS-ATRA$_{21}$ showed a selectively redox-sensitive ability. It could stay stable in low reducing environment such as extracellular parts and in normal cell. With the disassembly of the micelles meeting high levels of GSH in tumor cells, the drugs could consequently achieve rapid release and come into effect at the first time.

3.4. *Characterization of PTX-loaded micelles*

Following the same dialysis method, the PTX-loaded micelles with various DS of ATRA were prepared. Then, a series of characterization parameters, including DL, EE, particle size and zeta potential were measured and summarized in Table 2. The mean diameters of HA-SS-ATRA$_{21}$/PTX and HA-ATRA$_{20}$/PTX micelles were 114.5 nm and 119.6 nm with polydisperse index (PDI) of 0.097 and 0.114, respectively. This indicated that two kinds of micelles shared suitable and stable size. At the same time, TEM images were shown in Fig. 7 for a direct angle of the morphology and size of PTX-loaded micelles. Homogeneous and spherical micelles were seen in the figure. And the size was about 100 nm, which corresponded to that measured by DLS. Compared to the blank micelles, PTX-loaded micelles

Table 2 – Characteristics of PTX-loaded HA-SS-ATRA and HA-ATRA micelles (mean ± SD, $n = 3$).

Sample	EE[a] (%)	DL[b] (%)	Size[c] (nm)	PDI[d] (μ_2/Γ^2)	*Zeta* potential (mV)
HA-SS-ATRA$_8$ micelles[e]	89.48 ± 1.62	13.67 ± 1.01	126.8 ± 3.0	0.126 ± 0.031	−32.2 ± 1.8
HA-SS-ATRA$_{14}$ micelles[e]	91.78 ± 1.01	20.64 ± 0.87	123.7 ± 3.9	0.102 ± 0.024	−31.2 ± 2.3
HA-SS-ATRA$_{21}$ micelles[e]	92.64 ± 2.10	32.62 ± 1.39	114.5 ± 2.5	0.097 ± 0.038	−33.0 ± 1.4
HA-ATRA$_{20}$ micelles[e]	95.13 ± 1.87	31.14 ± 1.24	119.6 ± 3.0	0.114 ± 0.019	−35.5 ± 1.7

[a] EE are short for entrapment efficiency.
[b] DL are short for drug-loading.
[c] Mean diameters of micelles.
[d] Polydispersity index of micelles size.
[e] The number represents the DS of ATRA.

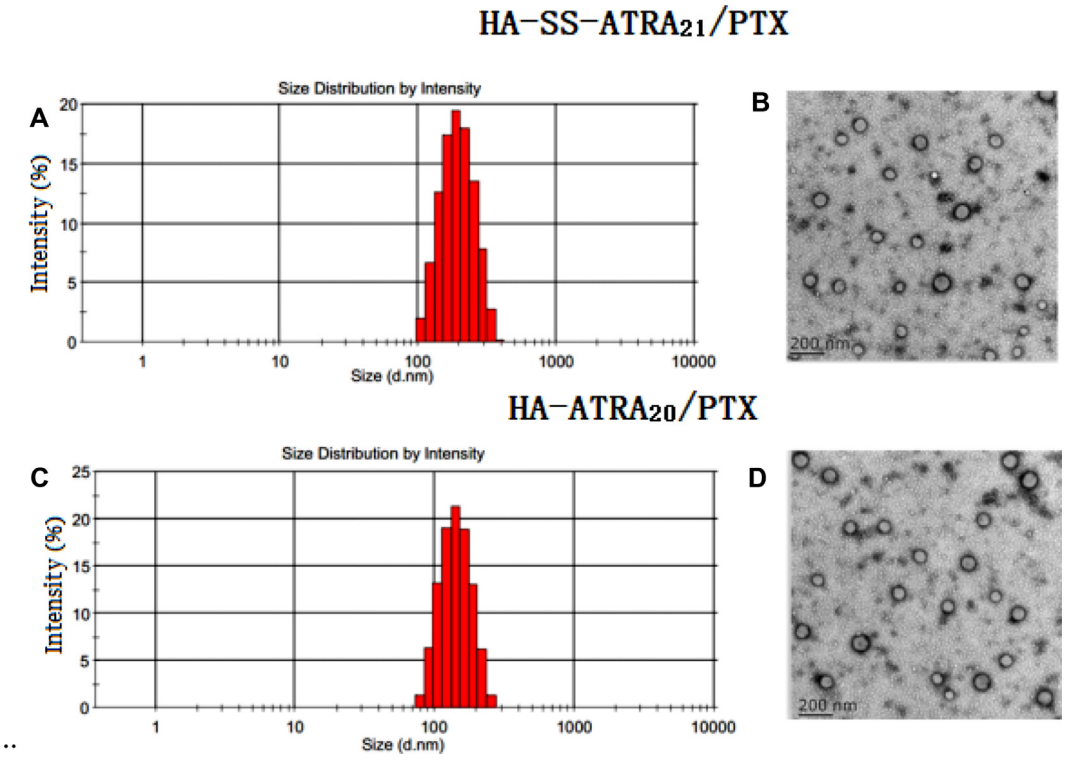

Fig. 7 – The DLS (A, C) and TEM (B, D) of HA-SS-ATRA$_{21}$/PTX micelles and HA-ATRA$_{20}$/PTX micelles.

displayed a smaller size and the size also got smaller as the DS of ATRA increased. Similarly, this could be explained by the hydrophobic interaction between ATRA and PTX, resulting in the closer core. Also, the zeta potential of PTX-loaded micelles around −32 mV was negative enough for the stability of micelles due to carboxyl groups of HA. DL and EE were further raised as the DS of ATRA in HA-SS-ATRA conjugates increased. One possibility was that, compared to other amphiphilic HA micelles, their hydrophobic tails are mostly fat chains, like PLGA [33], PCL [34] and C18 [35], since ATRA has a long conjugate structure, it may be important for it to form a molecule fence through not only hydrophobic interaction but also π–π stacking interaction [36], thus increasing the drug encapsulation efficiency and stability. For example, the best HA-SS-ATRA$_{21}$ micelles showed the excellent PTX DL of 32.62% and EE of 92.64%, ensuring the better drug efficacy. As control, HA-ATRA$_{20}$ micelles also displayed similar properties due to analogous structure.

XRD analyses, a classic method to recognize the structure and morphology of the materials, were carried out for PTX, blank HA-SS-ATRA$_{21}$ micelles, physical mixture and HA-SS-ATRA$_{21}$/PTX micelles. As shown from the XRD diagrams in Fig. 8, the blank micelles showed no obvious peak and PTX showed six characteristic peaks at 5.65°, 9.15°, 9.95°, 11.13°, 12.70°, 13.95° and numerous small peaks between 15°and 29°, which also existed in the figure of the physical mixture of blank HA-SS-ATRA$_{21}$ micelles and PTX, instead of in HA-SS-ATRA$_{21}$/PTX micelles. These results suggested that PTX was fully encapsulated into the core of the micelles and could not be detected by XRD.

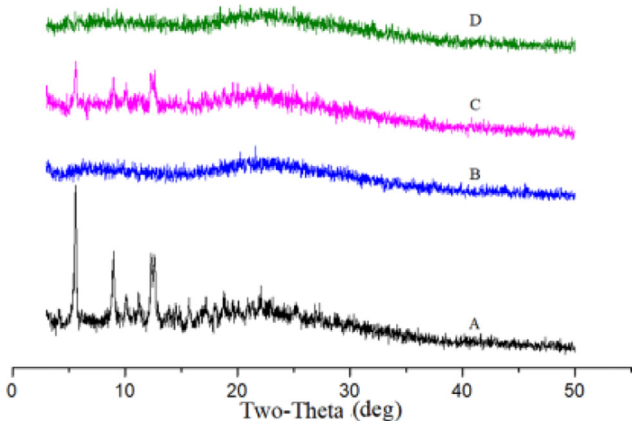

Fig. 8 – X-ray diffraction patterns of PTX (A), blank HA-SS-ATRA$_{21}$ micelles (B), physical mixture of HA-SS-ATRA$_{21}$ micelles and PTX (C), HA-SS-ATRA$_{21}$/PTX micelles (D).

3.5. *In vitro PTX and ATRA release triggered by GSH*

To mimic the reducing environment in different parts of the body, the drug release behavior was processed at different concentrations of GSH to observe the redox responsive release of both PTX and ATRA. Fig. 9 exhibited the release of PTX and ATRA from micelles in PBS (pH 7.4, 10 mM, 0.1% Tween 80) at 37°C with or without GSH. It was observed that the release of PTX and ATRA from HA-SS-ATRA$_{21}$/PTX was inefficient and slow in 10 μM GSH and no GSH. For example, only 9.5% of PTX was released at 6 h in the presence of 10 μM GSH, and only 8.0% without GSH. Furthermore, 15.5% of PTX and 12.3% of PTX were released within 24 h respectively, but nearly no ATRA were observed even within 24 h in 10 μM GSH and no GSH. However, once the concentration of GSH increased to 10 mM, it could be obviously found a rapid drug release. Specifically, about 26.9% of PTX and 9.8% of ATRA were released in 6 h, 46.1% of PTX and 32.1% of ATRA were released within 24 h. When the GSH concentration reached 20 mM, which was reported almost the same as in tumor cells [18], nearly 52.2% of PTX and 18.3% of ATRA were released within 6 h and approximately 91.4% and 56.8% were released within 24 h, respectively. The cumulative release of ATRA was lower than PTX in different concentration of GSH, this might be explained for covalently combination of ATRA on the conjugate, so it need firstly breakage from the conjugate chain and then the continuous diffusion, which is a little bit complicated than PTX. It should be further noted that the non-redox-sensitive HA-ATRA micelles exhibited a slow release of two drugs whatever the concentration of GSH. All these data implied that HA-SS-ATRA conjugates could reach a redox-responsive drug release most in tumor cells, which is valuable to protect normal cells and treat cancer.

3.6. *Cellular uptake studies*

To confirm the intracellular uptake ability of the micelles coated with HA, which possessed a high affinity to several malignant tumors overexpressing CD44 receptors. We chose NR to substitute PTX for its sensitive fluorescent signal as a marker to reveal the direct fluorescent intensity difference among experiment groups. We investigated the uptake of NR-loaded micelles in B16F10 cell line and L929 cell line. It is reported that the B16F10 tumor cells showed a high level of CD44 expression, while L929 cells show a low level [37].

In Fig. 10A, NR-loaded HA-SS-ATRA$_{21}$ micelles in B16F10 cells showed the highest fluorescence intensity, which may result from the rapid and efficient internalization through HA-CD44 mediated endocytosis. The group of NR-loaded HA-SS-ATRA$_{21}$ micelles treated with free HA further confirmed this point. Once HA receptors were occupied, it would certainly hinder the following uptake of the HA-coated micelles. Similarly, in the CD44-low-expression L929 cells, relatively weaker fluorescent of NR was observed in Fig. 10B. On the other hand, fluorescence intensity in B16F10

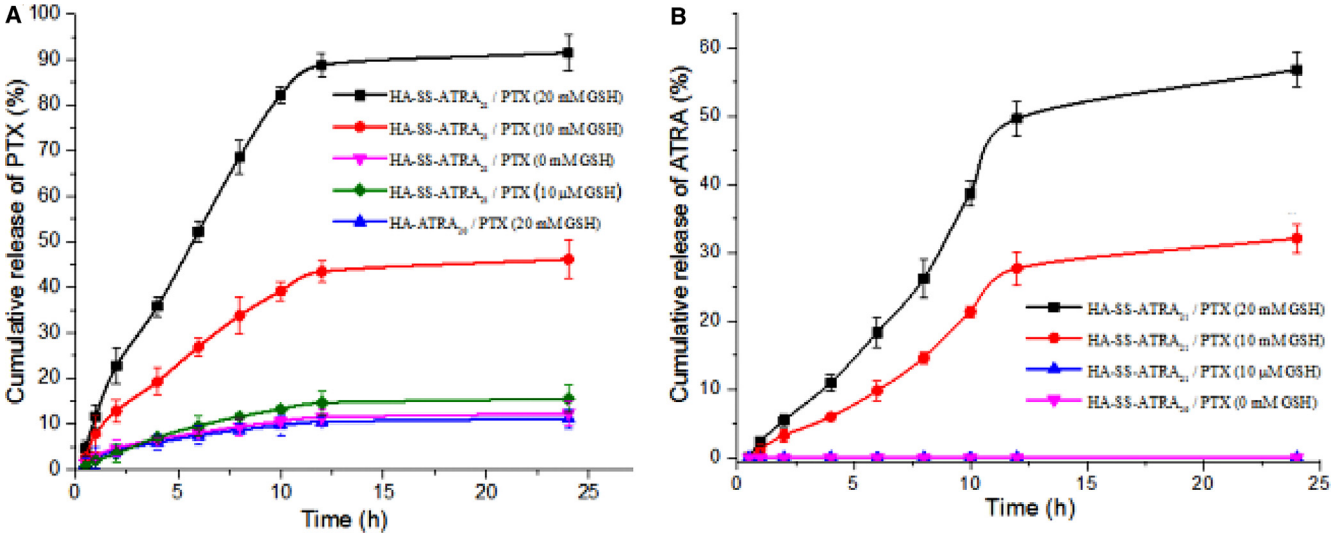

Fig. 9 – GSH triggered PTX and ATRA release from HA-SS-ATRA$_{21}$/PTX micelles and HA-ATRA$_{20}$/PTX micelles. The error bars in the graph represent standard deviations (n = 3).

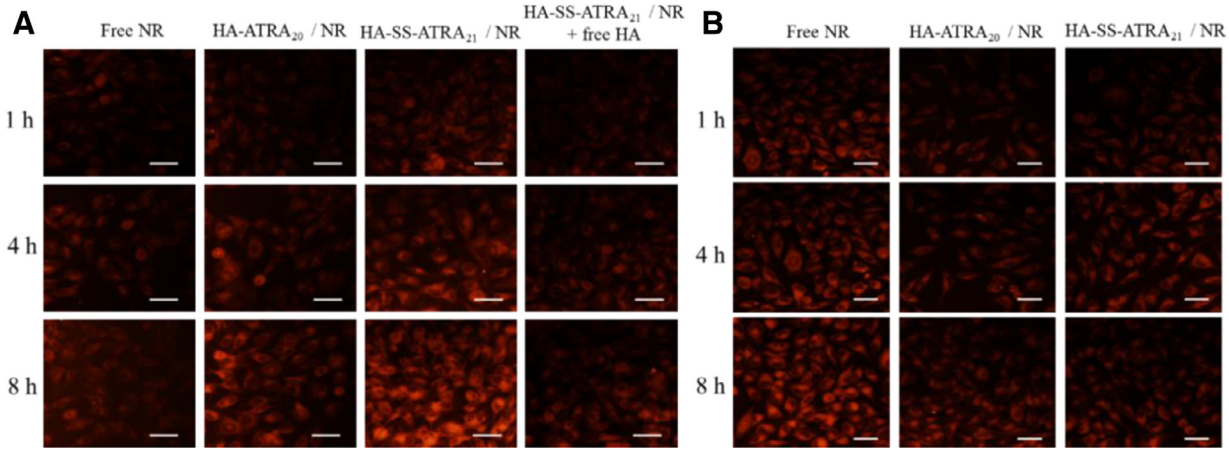

Fig. 10 – Fluorescent inverted microscope images of B16F10 cells (A) and L929 normal cells (B) incubation with NR-loaded HA-SS-ATRA$_{21}$ micelles and HA-ATRA$_{20}$ micelles, respectively. Scale bars correspond to 50 μm in all the images.

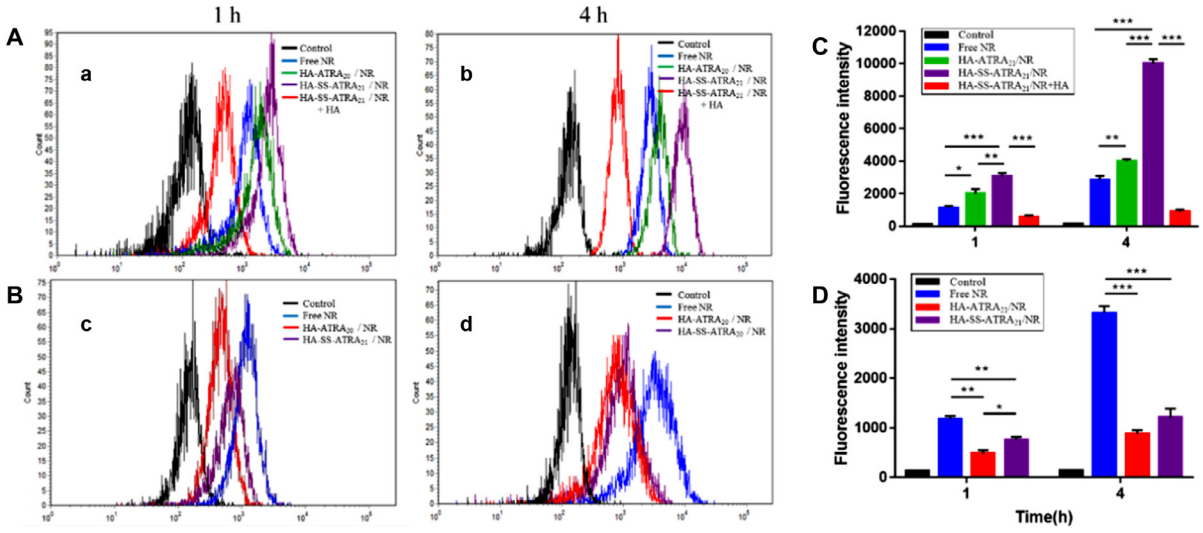

Fig. 11 – Flow cytometry analysis of free NR, HA-ATRA$_{20}$/NR micelles, HA-SS-ATRA$_{21}$/NR micelles and HA-SS-ATRA$_{21}$/NR micelles + free HA in B16F10 cells (A) at 1 h and 4 h; free NR, HA-ATRA$_{20}$/NR micelles and HA-SS-ATRA$_{21}$/NR micelles HA in L929 cells (B) at 1 h and 4 h. The corresponding data graph analysis of B16F10 cells (C) and L929 cells (D). *P < 0.1, **P < 0.05, ***P < 0.01.

cells were in the order of HA-SS-ATRA$_{21}$/NR micelles > HA-ATRA$_{20}$/NR micelles > free NR > HA-SS-ATRA$_{21}$/NR micelles treated with free HA. In contrast, fluorescence intensity of free NR in L929 cells is the highest. These results indicated that HA-CD44 receptor-mediated endocytosis is beneficial to promoting the uptake of HA-coated micelles in CD44 overexpressed cells. However, if CD44 is low expressed, these micelles would on the contrary delay the uptake compared to free drugs. Meanwhile, fluorescence intensity of HA-SS-ATRA$_{21}$/NR micelles in B16F10 cells was higher than HA-ATRA$_{20}$/NR micelles because the reducing environment inside B16F10 cells led to the disulfide breaking and drug release. A time-dependent change in fluorescence intensity were also observed, fluorescence intensity of all samples at 8 h were higher than 1 h. While in the case of L929 cells, its low expression of CD44 receptors decreased the uptake of NR, making the fluorescence of free NR appearing highest.

To further evaluate the cellular uptake of NR quantitatively, intracellular NR concentrations after different treatments were determined by flow cytometry. As shown in Fig. 11A and B, the results of FCM were consistent with the fluorescent inverted microscope observation. The intracellular NR concentrations are in the order of HA-SS-ATRA$_{21}$/NR micelles > HA-ATRA$_{20}$/NR micelles > free NR > HA-SS-ATRA$_{21}$/NR micelles treated with free-HA in B16F10 cells, while fluorescence intensity of free NR in L929 cells are the highest. Fig. 11C and D showed that there is a significant difference between free HA and HA-coated micelles, HA (+) and HA (−) pretreatment in B16F10 cells. In L929 cells, cellular uptake of free NR is much higher than HA-coated micelles, this may

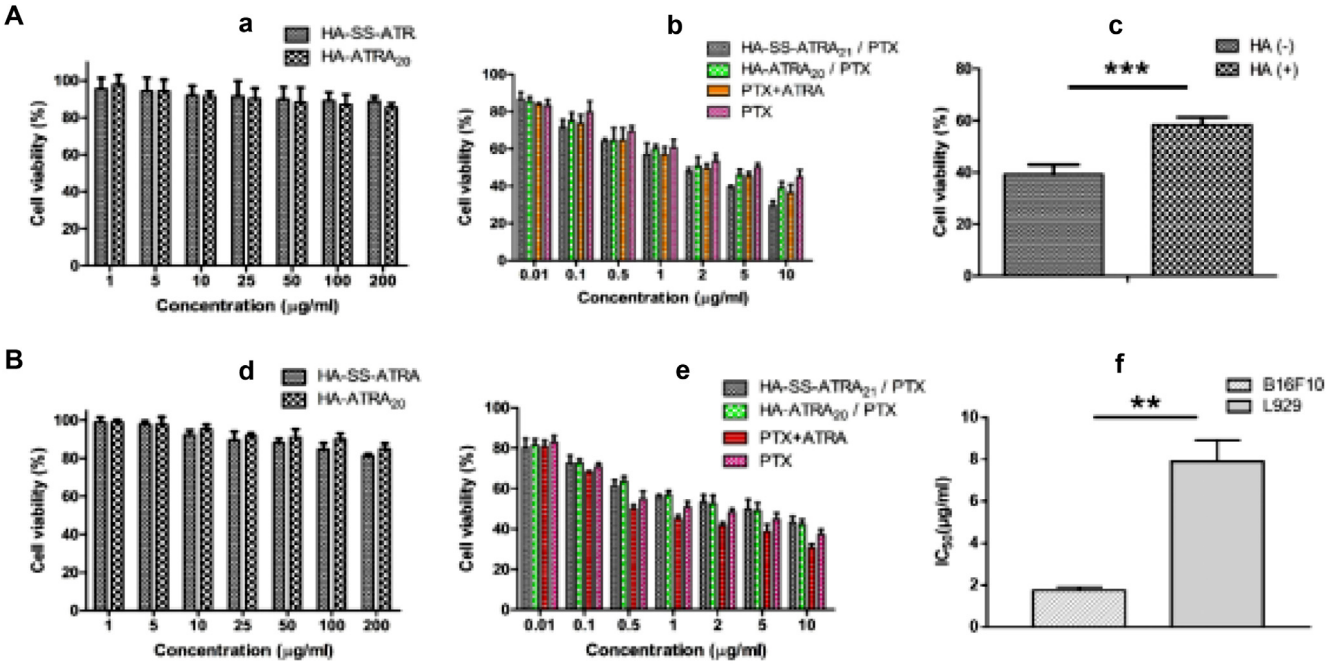

Fig. 12 – Cytotoxicity of two blank micelles (a, d), HA-SS-ATRA$_{21}$/PTX micelles, HA-ATRA$_{20}$/PTX micelles, PTX and PTX + ATRA (b, e) against B16F10 cells (A) and L929 cells (B), HA-SS-ATRA$_{21}$/PTX in the presence (+) or absence (–) of free HA (c) against B16F10 cells (A), comparison of IC$_{50}$ of HA-SS-ATRA$_{21}$/PTX micelles against B16F10 and L929 (f). Results were expressed as the mean ± SD from three independent experiments. **$P < 0.05$, ***$P < 0.01$.

result from the low expression of CD44 receptors on L929 and instead, hinders the cellular uptake. Therefore, it will be more convinced to demonstrate the HA-CD44 interaction-mediated cellular uptake.

3.7. *In vitro cytotoxicity studies*

Generally speaking, excellent properties of high cellular uptake, rapid release and combination therapy can bring higher cytotoxicity. To prove these three points combined together in the redox-sensitive HA-SS-ATRA$_{21}$/PTX, the *in vitro* antitumor activity of HA-SS-ATRA$_{21}$/PTX micelle, HA-ATRA$_{20}$/PTX micelle, PTX and PTX + ATRA were evaluated in B16F10 cancer cells and L929 cells.

As shown in Fig. 12, a higher cytotoxicity of PTX + ATRA solution compared to PTX solution both against B16F10 and L929 cells, which suggested ATRA can enhance the cytotoxicity of PTX. Blank HA-SS-ATRA$_{21}$ and HA-ATRA$_{20}$ micelles showed little cytotoxicity against both B16F10 and L929 cells even at high concentrations, suggesting that the material was well biocompatible.

Interestingly, HA-SS-ATRA$_{21}$/PTX micelles showed higher anticancer activity against CD44-positive B16F10 cells among the four groups, while PTX + ATRA showed higher anticancer activity against CD44-negative L929 cells. This was because HA-SS-ATRA$_{21}$/PTX micelles could target CD44-positive cells by CD44 receptor-mediated endocytosis. Meanwhile, HA-SS-ATRA$_{21}$/PTX micelles showed strengthened antitumor activity against CD44-positive B16F10 cells compared to HA-ATRA/PTX micelles, which resulted from increased release of drugs. Furthermore, cell viability was increased when the CD44 receptor was saturated by pretreatment with free HA as shown in Fig. 12A(c). Meanwhile, in Fig. 12B(f), we found that HA-SS-ATRA micelles displayed significant difference in the IC$_{50}$ between B16F10 and L929 cells (B16F10 IC$_{50}$ 1.75 ± 0.16 μg/ml, L929 IC$_{50}$ 7.90 ± 1.02 μg/ml). These results further confirmed the active targeting efficiency of HA-SS-ATRA/PTX micelles through CD44 receptor-mediated endocytosis, which were in agreement with the results of fluorescence microscopy and FCM analyses.

3.8. *Pharmacokinetics*

It is important for the combination chemotherapy drugs to keep stable and achieve prolonged circulation in the bloodstream before reaching to the tumor sites after intravenous injection [38]. To depict the pharmacokinetic characteristics of HA-SS-ATRA$_{21}$/PTX and HA-ATRA$_{20}$/PTX, pharmacokinetic studies were conducted at the PTX dose of 7 mg/kg in SD rats, and Taxol® as control. The plasma drug concentration-time curves of PTX were presented in Fig. 13. It is easy to find that the Taxol® was quickly cleared from the plasma and could hardly be monitored at above 8 h. In contrast, HA-SS-ATRA$_{21}$/PTX and HA-ATRA$_{20}$/PTX displayed a prolonged blood circulating effect in plasma, and PTX was still detectable after administration for 48 h. The main pharmacokinetic parameters of PTX were calculated by BAPP2.0 using a non-compartmental model and were listed in Table 3. The HA-SS-ATRA$_{21}$/PTX and HA-ATRA$_{20}$/PTX significantly increased MRT of PTX by 6.53-fold and 6.81-fold, with a corresponding significantly decrease in CL ($P < 0.01$), respectively. Besides, compared to Taxol®, the AUC$_{0-t}$ of HA-SS-ATRA$_{21}$/PTX and

Table 3 – Non-compartmental analysis of plasma data for PTX in rats after i.v. administration of HA-SS-ATRA$_{21}$/PTX, HA-ATRA$_{20}$/PTX and Taxol® (mean ± SD, n = 5).

Pharmacokinetic parameters	HA-SS-ATRA$_{21}$/PTX	HA-ATRA$_{20}$/PTX	Taxol®
AUC_{0-t} (h.μg/ml)	36.86 ± 5.64**	34.07 ± 1.29**	4.02 ± 0.06
$T_{1/2}$ (h)	69.11 ± 24.30	108.44 ± 73.95	8.49 ± 1.32
MRT (h)	20.95 ± 1.29**	21.86 ± 0.46**	3.21 ± 0.02
CL (ml/h/kg)	55.84 ± 30.80**	35.59 ± 13.64**	649.48 ± 31.50
V_d (ml/kg)	5250.93 ± 112.98	6278.07 ± 656.18	7910.78 ± 886.69

** $P < 0.01$ *versus* Taxol.

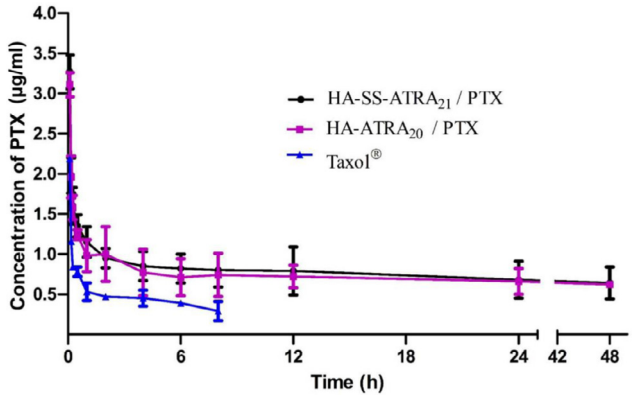

Fig. 13 – Plasma concentration-time profiles of PTX in rats following intravenous administration of HA-SS-ATRA$_{21}$/PTX, HA-ATRA$_{20}$/PTX and Taxol® (7 mg/kg) (mean ± SD, n = 5).

HA-ATRA$_{20}$/PTX were increased by 9.17-fold and 8.48-fold, respectively. The results further indicated that HA-SS-ATRA$_{21}$/PTX and HA-ATRA$_{20}$/PTX could put off the elimination of PTX and prolong its circulation time in bloodstream, which was attributed to suitable particle size, high negative charge and hydrophilic surface of HA.

4. Conclusion

In the present, we designed and synthesized a biodegradable amphiphilic HA-SS-ATRA conjugate, which possessed high DS of ATRA and low CMC. The micelles exhibited excellent DL capacities both for PTX and ATRA, with suitable particle size and micellar stability. Importantly, HA-SS-ATRA$_{21}$/PTX micelles exhibited an obvious redox-sensitive and burst release of PTX and ATRA *in vitro* drug release studies. Moreover, CD44 receptor-mediated tumor targeting potential could significantly enhance micelles accumulation in tumor site, where high concentration of GSH led to rapid drug release. Due to the combination mode of PTX and ATRA, using ATRA as parts of the carriers to entrap PTX not only protect the inner drug, but can also improve the cytotoxicity in tumor cells. All in all, the constructed redox-sensitive HA-SS-ATRA micelles can be used as drug carriers of PTX and ATRA with the ability of controlled internalization release and active tumor-targeting for cancer combination chemotherapy.

Conflicts of interest

The authors report no conflicts of interest.

Acknowledgments

This work was financially supported by the National Natural Science Foundation of China (Grant Nos. 81703382 and 81673567). The authors are thankful to Lei Chen for animal experiment guide and Yanfeng Hao for cell experiment guide.

REFERENCES

[1] William NH. Drug resistance. Boston, MA: Springer; 1996.
[2] Hu CJ, Zhang L. Nanoparticle-based combination therapy toward overcoming drug resistance in cancer. Biochem Pharmacol 2012;83(8):1104–11.
[3] Rowinsky EK, Onetto N, Canetta RM, Arbuck SG. Taxol: the first of the taxanes, an important new class of antitumor agents. Semin Oncol 1992;19(6):646–62.
[4] Tiersten AD, Selleck MJ, Hershman DL, et al. Phase II study of topotecan and paclitaxel for recurrent, persistent, or metastatic cervical carcinoma. Gynecol Oncol 2004;92(2):635–8.
[5] Ueda Y, Yamagishi H, Ichikawa D, et al. Multicenter phase II study of weekly paclitaxel plus S−1 combination chemotherapy in patients with advanced gastric cancer. Gastric Cancer 2010;13(3):149–54.
[6] Fader AN, Nagel C, Axtell AE, et al. Stage II uterine papillary serous carcinoma: carboplatin/paclitaxel chemotherapy improves recurrence and survival outcomes. Gynecol Oncol 2009;112(3):558–62.
[7] Kato J, Nagahara A, Iijima K, et al. Phase I study of paclitaxel, cisplatin and 5-fluorouracil combination chemotherapy for unresectable/recurrent gastric cancer. Adv Med Sci – Poland 2010;55(2):137–42.
[8] Sun J, Huang H, Zhu Y, et al. The expression of telomeric proteins and their probable regulation of telomerase during the differentiation of all-trans-retinoic acid-responsive and -resistant acute promyelocytic leukemia cells. Int J Hematol 2005;82(3):215–23.
[9] Pratt MA, Niu MY, Renart LI. Regulation of survivin by retinoic acid and its role in paclitaxel-mediated cytotoxicity in MCF-7 breast cancer cells. Apoptosis 2006;11(4):589–605.
[10] Karmakar S, Banik NL, Ray SK. Combination of all-trans retinoic acid and paclitaxel-induced differentiation and apoptosis in human glioblastoma U87MG xenografts in nude mice. Cancer – Am Cancer Soc 2008;112(3):596–607.
[11] Bae Y, Diezi TA, Zhao A, Kwon GS. Mixed polymeric micelles for combination cancer chemotherapy through the

concurrent delivery of multiple chemotherapeutic agents. J Control Release 2007;122(3):324–30.
[12] Sokolsky-Papkov M, Agashi K, Olaye A, Shakesheff K, Domb AJ. Polymer carriers for drug delivery in tissue engineering. Adv Drug Deliv Rev 2007;59(4–5):187–206.
[13] Fang J, Nakamura H, Maeda H. The EPR effect: unique features of tumor blood vessels for drug delivery, factors involved, and limitations and augmentation of the effect. Adv Drug Deliv Rev 2011;63(3):136–51.
[14] Ikada Y, Tsuji H. Biodegradable polyesters for medical and ecological applications. Macromol Rapid Commun 2000;21(3):117–32.
[15] Shuai X, Ai H, Nasongkla N, Kim S, Gao J. Micellar carriers based on block copolymers of poly(epsilon-caprolactone) and poly(ethylene glycol) for doxorubicin delivery. J Control Release 2004;98(3):415–26.
[16] Cheng R, Feng F, Meng F, Deng C, Feijen J, Zhong Z. Glutathione-responsive nano-vehicles as a promising platform for targeted intracellular drug and gene delivery. J Control Release 2011;152(1):2–12.
[17] Meng F, Hennink WE, Zhong Z. Reduction-sensitive polymers and bioconjugates for biomedical applications. Biomaterials 2009;30(12):2180–98.
[18] Gilbert HF. Thiol/disulfide exchange equilibria and disulfide bond stability. Methods Enzymol 1995;251(1):8–28.
[19] Raina S, Missiakas D. Making and breaking disulfide bonds. Annu Rev Microbiol 1997;51(1):179–202.
[20] Balendiran GK, Dabur R, Fraser D. The role of glutathione in cancer. Cell Biochem Funct 2004;22(6):343–52.
[21] Schafer FQ, Buettner GR. Redox environment of the cell as viewed through the redox state of the glutathione disulfide/glutathione couple. Free Radic Biol Med 2001;30(11):1191–212.
[22] Wen HY, Dong HQ, Xie WJ, et al. Rapidly disassembling nanomicelles with disulfide-linked PEG shells for glutathione-mediated intracellular drug delivery. Chem Commun (Camb) 2011;47(12):3550–2.
[23] Kuppusamy P, Li H, Ilangovan G, et al. Noninvasive imaging of tumor redox status and its modification by tissue glutathione levels. Cancer Res 2002;62(1):307–12.
[24] Saravanakumar G, Deepagan VG, Jayakumar R, Park JH. Hyaluronic acid-based conjugates for tumor-targeted drug delivery and imaging. J Biomed Nanotechnol 2014;10(1):17–31.
[25] Vafaei SY, Esmaeili M, Amini M, Atyabi F, Ostad SN, Dinarvand R. Self-assembled hyaluronic acid nanoparticles as a potential carrier for targeting the inflamed intestinal mucosa. Carbohyd Polym 2016;144(25):371–81.
[26] Xu X, Jha AK, Harrington DA, Farach-Carson MC, Jia X. Hyaluronic acid-based hydrogels: from a natural polysaccharide to complex networks. Soft Matter 2012;8(12):3280–94.
[27] Cho HJ, Yoon HY, Koo H, et al. Self-assembled nanoparticles based on hyaluronic acid-ceramide (HA-CE) and Pluronic® for tumor-targeted delivery of docetaxel. Biomaterials 2011;32(29):7181–90.
[28] Herrlich P, Sleeman J, Wainwright D, et al. How tumor cells make use of CD44. Cell Adhes Commun 1998;6(2-3):141–7.
[29] Hall CL, Yang B, Yang X, et al. Overexpression of the hyaluronan receptor RHAMM is transforming and is also required for H-ras transformation. Cell 1995;82(1):19–26.
[30] Li J, Huo M, Wang J, et al. Redox-sensitive micelles self-assembled from amphiphilic hyaluronic acid-deoxycholic acid conjugates for targeted intracellular delivery of paclitaxel. Biomaterials 2012;33(7):2310–20.
[31] Yao J, Zhang L, Zhou J, Liu H, Zhang Q. Efficient simultaneous tumor targeting delivery of all-trans retinoid acid and paclitaxel based on hyaluronic acid-based multifunctional nanocarrier. Mol Pharm 2013;10(3):1080–91.
[32] Miller T, Rachel R, Besheer A, Uezguen S, Weigandt M, Goepferich A. Comparative investigations on *in vitro* serum stability of polymeric micelle formulations. Pharm Res-Dordr 2012;29(2):448–59.
[33] Huang J, Zhang H, Yu Y, et al. Biodegradable self-assembled nanoparticles of poly (D,L-lactide-co-glycolide)/hyaluronic acid block copolymers for target delivery of docetaxel to breast cancer. Biomaterials 2014;35(1):550–66.
[34] Han HS, Thambi T, Choi KY, et al. Bioreducible shell-cross-linked hyaluronic acid nanoparticles for tumor-targeted drug dlivery. Biomacromolecules 2015;16(2):447–56.
[35] Liu Y, Sun J, Lian H, Cao W, Wang Y, He Z. Folate and CD44 receptors dual-targeting hydrophobized hyaluronic acid paclitaxel-loaded polymeric micelles for overcoming multidrug resistance and improving tumor distribution. J Pharm Sci-US 2014;103(5):1538–47.
[36] Paton RS, Goodman JM. Hydrogen bonding and pi-stacking: How reliable are force fields? A critical evaluation of force field descriptions of nonbonded interactions. J Chem Inf Model 2009;49(4):944–55.
[37] Eliaz RE, Szoka FC. Liposome-encapsulated doxorubicin targeted to CD44. Cancer Res 2001;61(6):2592–601.
[38] Choi KY, Min KH, Yoon HY, et al. PEGylation of hyaluronic acid nanoparticles improves tumor targetability *in vivo*. Biomaterials 2011;32(7):1880–9.